Volume 1 | Number 1 | Jan 2013 | Pages 1–100

Journal of
Materials Chemistry A

Materials for energy and sustainability
www.rsc.org/materialsA

Li⁺

e⁻

ROYAL SOCIETY
OF CHEMISTRY

ROYAL SOCIETY
OF CHEMISTRY

www.rsc.org/materialsA

High Supercapacitor and Adsorption Behaviors of Flower-like MoS$_2$ nanostructures

Xiuhua Wang*, Juanjuan Ding, Shangwu Yao, Xiaoxiu Wu, Qingqing Feng,

Zhenghua Wang*，Baoyou Geng*

The Key Laboratory of Functional Molecular Solids, Ministry of Education, College of Chemistry and Materials Science, Anhui Normal University, Wuhu 241000, China

Abstract

Uniform 3D flower-like MoS$_2$ nanostructures were successfully synthesized through a facile two-step hydrothermal method and were applied as electrode material for high-performance electrochemical capacitors. Galvanostatic charge–discharge measurements showed that the MoS$_2$ electrode had a specific capacitance of 168 F g^{-1} at a current density of 1 A g^{-1} and still retaining 92.6% after the 3000 cycles. Furthermore, the as-prepared MoS$_2$ nanostructures were used as an adsorbent in Rhodamine B aqueous solution, and the maximum adsorption capacity toward Rhodamine B was about 49.2 mg g^{-1}.

Keywords: Flower-like MoS$_2$; Electrochemical capacitors; Adsorbent

1. Introduction

Transition metal sulfides have attracted great attention in a variety of fields, such as lithium-ion batteries (LIBs),[1] Electrochemical capacitors (ECs),[2, 3] potential hydrogen storage, catalyst and solid lubricant,[4, 5] owing to their unique crystal structure and chemical properties. As one of the representative members, MoS$_2$ has received much attention in many fields due to its unique atomic structure. MoS$_2$ is composed of three atom layers (covalently bound S–Mo–S trilayer), and the triple layers are stacked and held together by weak van der Waals interactions.[6, 7] Because of the weak van der Waals interactions, MoS$_2$ can be exfoliated to a single-layer or few-layers structure easily, which is the analogue of graphene.[8, 9]

As is well known, graphene materials have been extensively applied in areas of photoelectricity, electrics and supercapacitor, because of their high electrical conductivity and great chemical stability.[10, 11] However, graphene is generally

expensive. Unlike graphene, MoS_2 nanostructure can be easily synthesized at large scale with low cost techniques such as hydrothermal, chemical vapor deposition and sonochemical routes.[12-14] Moreover, the two-dimensional (2D) electron correlations among Mo atoms could improve the properties of complicated planar electric transportation. It is expected that this material could be a substitute for graphene in many fields such as ECs, adsorbents, and so on.

In recent years, ECs have become a new research hot spot in the field of energy storage due to its high levels of electrical power, large specific energy density, fast charging–discharging rates and environmental protection.[15, 16] According to the working mechanisms, supercapacitors can be divided into two types. One is pseudocapacitors which is a Faradic process relying on redox reactions, usually containing transition metal oxides or hydroxides and conducting polymers as electrode materials.[17] The other is electric double layer capacitors (EDLCs) due to charge separation at the electrolyte interface, such as carbon nanospheres, carbon nanotubes and graphene.[18, 19] Nowadays, MoS_2 has attracted more attention in supercapacitors because of its higher intrinsic ionic conductivity than oxides and higher theoretical capacity than graphite.[20, 21]

Until now, to the best of our knowledge, reports on supercapacitors behavior of pure MoS_2 are still limited.[22] Soon et al. exhibited MoS_2 based micro-supercapacitor with a capacitance of 8 mF cm^{-2} (volumetric capacitance of 178 F cm^{-3}).[22] Sun et al. reported porous tubular C/MoS_2 nanocomposites and the bulk MoS_2 with capacitance of 210 and 40 F g^{-1} at 1 A g^{-1}, respectively.[23] Huang et al. demonstrated polyaniline/2-dimensional graphene analog MoS_2 composites for high-performance supercapacitor and the specific capacitances of the pure MoS_2 electrodes was only 98 F g^{-1} at 1 A g^{-1}.[24] Recently, Kim and co-workers synthesized MoS_2 nanostructures through a hydrothermal method and used as the anode material in 1 M Na_2SO_4 aqueous electrolyte. However, the electrochemical tests showed that the maximum specific capacity was just about 92.85 F g^{-1} at a constant discharge current density of 0.5 mA cm^{-2}.[25] Ma et al. reported the flower-like MoS_2 nanospheres synthesized by a hydrothermal route and the specific capacitance of MoS_2 is 122 F g^{-1} at 1 A g^{-1}.[26]

With the development of industrialization, water pollution has attracted intensive concern. Among the various pollutants, the pollution of water resources by dyes from the textile has become a serious environmental problem. In order to remove the dyes from the aqueous environment, numerous methods have been explored, such as adsorption, photocatalysis, electrochemical degradation, acidification, etc.[27] Among the above-mentioned methods, adsorption technology has been applied extensively to remove organic pollutants from aqueous solutions due to its simplicity, speed, low cost, high removal capacity, low secondary pollution and environmentally friendly nature.[28] Recently, three-dimensional (3D) transition metal oxide materials have been widely used as adsorbents to deal with organic dyes from waste water.[29, 30]

Herein, 3D flower-like MoS_2 nanostructures were synthesized through a facile two-step hydrothermal method by using MoO_3 nanorods as precursor. The as-prepared MoS_2 possess of a typical electrical double-layer capacitance. The MoS_2 electrode showed a high specific capacitance of 168 F g^{-1} at 1 A g^{-1} in 1 M KCl solution. In addition, the MoS_2 materials show excellent long-term cyclic stability. The capacitance still remains about 92.6% after 3000 cycles of charge–discharge at a current density of 1 A g^{-1}. Furthermore, the materials were used as adsorbent in Rhodamine B (RhB) solution and exhibited a strong capability to remove organic pollutants.

2. Experimental

2.1 Reagents

Ammonium molybdate ($(NH_4)_6Mo_7O_{24}$), thiourea (H_2NCSNH_2), nitric acid (HNO_3) and absolute ethanol were purchased from Sinopharm Chemical Reagent Co., Ltd. All these reagents were of analytical grade and used without further purification. Deionized water was used throughout.

2.2 Synthesis of MoO_3 nanostructures

The MoO_3 nanorods were synthesized as follows: 0.524 g $(NH_4)_6Mo_7O_{24}$ were dissolved in 30 mL deionized water under violent stirring for about 10 min. Then 10 mL 2.2 M HNO_3 solutions were transferred into the above solution. Finally, the

solution was transferred into a 50 mL Teflon-lined stainless steel autoclave and heated at 180 °C for 21 h. The product was rinsed several times with deionized water and absolute ethanol, and then was dried in vacuum at 60 °C for 24 h.

2.3 Synthesis of flower-like MoS_2 nanostructures

The MoS_2 nanostructures were synthesized by MoO_3 and H_2NCSNH_2. In short: 0.08 g H_2NCSNH_2 was dissolved in 30 mL deionized water. After stirring for 10 min, 0.08 g MoO_3 were added into the above solution with ultrasonic treatment for 10 min, and then the solution was violently stirred for about 20 min. Finally, the mixed solution was transferred into a 50 mL Teflon-lined stainless steel autoclave and heated at 180 °C for 40 h. The autoclave was allowed to cool naturally to room temperature. The product was collected by centrifugation, washed with distilled water and ethanol for several times and finally dried at 60 °C for 8 h.

2.4 Material characterization

The scanning electron microscopy (SEM) images have been taken with a Hitachi S-4800 field-emission scanning electron microscope. X-ray powder diffraction (XRD) patterns have been obtained on a Rigaku Max-2200 with Cu Kα radiation. The transmitting electron microscopy (TEM) images were recorded on a FEI Tecnai G^2 20 high-resolution transmission electron microscope performed at an acceleration voltage of 200 kV. The surface area of the as-obtained sample was computed from the results of N_2 physisorption at 77 K (model: BECKMANSA3100 COULTER) using the BET (Brunauer–Emmett–Teller) formalism. UV-vis absorption spectra were recorded on a Hitachi U-3010 spectrophotometer

2.5 Electrochemical measurements

The capacitive performances of the as-prepared MoS_2 sample were measured on a CHI 660D electrochemical working station (Chenhua Corp., Shanghai, China) with a three electrode experimental setup. The working electrode was made of as-prepared MoS_2 (80 wt %), acetylene black (15 wt %) and polytetrafluoroethylene (PTFE) binder (5 wt %). After grinding, the mixed materials were pasted onto a piece of nickel

foam and dried under vacuum at 60 °C for 3 h. Platinum wire and standard calomel electrode (SCE) were used as the counter and reference electrodes, respectively.

The specific capacitance (C) of the electrode can be evaluated according to the following equation (Eq.):

$$C = \frac{I \times \Delta t}{m \times \Delta V}$$

(1)

Where C (F g^{-1}) is the specific capacitance of the electrode based on the mass of active materials, I (A) is the current during discharge process, Δt (s) is the discharge time, ΔV (V) is the potential window, m (g) is the mass of active materials.

2.6 Adsorption behavior measurements of RhB

The Adsorption behavior of RhB was conducted according to the following procedure: 0.02 g of the as-prepared MoS_2 was respectively dispersed into 50 mL RhB solution of different concentrations (10, 15, 20, 25, 30 mg L^{-1}). Then the solution was placed in the dark and stirred vigorously with a magnetic stirrer. 4 mL of the suspension was taken out at every 5 mins. Finally the suspension was centrifuged and collected. The concentrations of RhB were analyzed at 553 nm with a UV-vis spectrometer. The adsorption capacity of the outcomes was calculated by the following Eq.:

$$Q_t = (C_0 - C_t)V/W$$

(2)

where Q_t (mg g^{-1}) is the adsorption capacity at different time, C_0 (mg L^{-1}) is the initial concentration of the RhB solution, C_t (mg L^{-1}) is the concentration of the RhB solution at time t of adsorption, V (L) is the volume of the RhB solution and W (g) is the weight of the adsorbent.

3. Results and discussion

3.1. Material characterization

The morphology of the as-prepared samples was studied by SEM. Figure 1(a) shows a SEM image of the precursor MoO_3 in which many nanorods with the average diameter of 400 nm and lengths up to 15 μm were seen. Figure 1(b) displays an X-ray powder diffraction (XRD) pattern of the MoO_3 nanorods. It can be seen that all of the

diffraction peaks can be perfectly indexed to pure MoO_3 (JCPDS card No. 47-1320) and no excrescent peaks are detectable.

The low-magnification SEM image (Fig. 2a) demonstrates that the typical product consists of a large quantity of uniform 3D flower-like nanostructures. The flower-like nanostructures have diameters of about 300–500 nm. The high-magnification SEM image (Fig. 2b) reveals that the flower-like nanostructures were composed of intercrossed curved nanoflakes with thickness of several nanometers. Transmission electron microscopic (TEM) observation further confirms the result of SEM. Figure 2(c) depicts a TEM image of an individual nanoflower, from which the intercrossed nanosheets with dense and smooth surfaces can be clearly seen. Figure 2(d) displays an XRD patterns of the final product, in which the diffraction peaks can be assigned to the (0 0 2), (1 0 0), (1 0 2), (0 0 6) and (1 1 0) planes of hexagonal MoS_2 (JCPDS No. 37-1492), respectively. And the crystallization of flower-like MoS_2 is similar to the previous reports.[23-26]

3.2. Growth mechanism

On the basis of the above experimental results and analysis, we propose a possible mechanism to explain the formation of the flower-like MoS_2 nanostructures. The following reactions may occur during the hydrothermal process:

$$6HNO_3 + (NH_4)_6Mo_7O_{24} = 7MoO_3 + NH_4NO_3 + 3H_2O \tag{3}$$

$$NH_2CSNH_2 + 2H_2O = 2NH_3 + H_2S + CO_2 \tag{4}$$

$$3MoO_3 + H_2S = 3MoS_2 + SO_2 + 7H_2O \tag{5}$$

At the initial stage, HNO_3 react with $(NH_4)_6Mo_7O_{24}$ under hydrothermal condition and white color MoO_3 is produced according to Eq. (3). At the second stage, NH_2CSNH_2 decomposed into H_2S gas at high temperature [Eq. (4)]. The produced H_2S react with MoO_3 and black color MoS_2 is produced [Eq. (5)]. According to the above reactions, the morphological evolution process of the MoS_2 nanostructures was presumed and illustrated in Scheme 1. Of course, it still needs more detailed and

systematic work to provide evidence to make clear the precise growth mechanism of the flower-like MoS_2 nanostructures.

3.3. Electrochemical properties

Cyclic voltammetry (CV) curves were measured at various scan rates ranging from 10 to 100 mV s^{-1} in 1 M KCl solution to reflect the electrochemical properties of MoS_2, as shown in Fig. 3a. It is obvious that there is no redox peaks in all CV curves, indicating that MoS_2 nanoflowers possess a typical electrical double-layer capacitance, which is similar to the previous reports. [24, 25]

Galvanostatic charge–discharge curves of the MoS_2 nanoflowers are investigated at various current densities (0.5, 1, 2 and 4 A g^{-1}) with voltage between −0.9 V and −0.2 V, as shown in Fig. 3b. During the charge–discharge process, all the curves are symmetric and present good supercapacitive behaviors. The specific capacitances are obtained from Eq. (1). According the results, the specific capacitances of the MoS_2 nanoflowers are 178, 168, 159 and 148 F g^{-1} at 0.5, 1, 2 and 4 A g^{-1}, respectively. In the previous research, the specific capacitances of the pure MoS_2 electrodes were only 40, 98, 122 F g^{-1} at 1 A g^{-1}, respectively.[23, 24, 26] The observed specific capacitance is high compared to the previous research, which is attributed to the uniform nanoflowers morphology.

For supercapacitors, cycling stability is also a very important parameter. Therefore, galvanostatic charge–discharge measurements of the MoS_2 nanoflowers for 3000 cycles are further conducted at a current density of 1 A g^{-1} with a potential window of −0.7 V, as shown in Figure 3c. The result shows that there is only a slight decrease and the capacitance still remains about 92.6% after 3000 cycles, demonstrating that MoS_2 nanoflowers have good cycling stability.

Electrochemical impedance measurements were also applied for the MoS_2 nanoflowers, as shown in Fig. 3d. Clearly, the Nyquist plots before and after 100 cycles are composed of a semicircle at the high frequency region and a straight line at the low frequency region. The semicircle in the high frequency range is attributed to the three sections: electrolyte, electroactive material and the contact resistance between the

electroactive material and the current collector, and the straight line is related to the diffusive resistance. There is no obvious difference between the 1st and 100 st cycles, indicating that MoS_2 nanoflowers are suitable for supercapacitors.

3.4 Application in waste water treatment

Figure 4a shows the absorption spectra of 20 mg L^{-1} RhB solution with 0.02 g as-prepared MoS_2 at different times in the adsorption process. The characteristic absorption peaks of RhB at 553 nm were used to monitor the adsorption process. After 5 mins of adsorption, the original concentration has been decreased for 78%, and RhB can be completely removed within 35 mins. Fig. 4b displays the variations of RhB concentration (C/C_0) over the whole adsorption process. It is obvious that the adsorption reached equilibrium after 35 min, and more than 91% RhB molecules were adsorbed.

Figure 4c shows the adsorption isotherms of RhB solution, indicating that the values of Qe increase with the increase of the RhB concentration, and reaches a maximum value when the RhB concentration is too high. The experimental data consistent with the Langmuir adsorption model isotherms. According to this isotherm, the maximum adsorption capacity of the MoS_2 nanoflowers is about 49.2 mg g^{-1}. These data indicate that the MoS_2 nanoflowers possess good adsorption capacities on RhB solution.

As we know, the surface structure of the adsorbent and the intermolecular force between the material surface and the dye species are responsible for the dye removal. RhB adsorption typically takes place because of the electrostatic attraction between its cationic groups and the charges on the surface or the sorbent as well as the surface area and pore size of the material. BET surface area of the flower-like MoS_2 is 18.68 $m^2 g^{-1}$, as shown in Fig. 4d, and the size of the average pore width is about 16.8 nm (inset of Fig. 4d). The BET surface area of flower-like MoS_2 is not very large, so the adsorption capacity may not be concerned with the surface area. And the high adsorption ability maybe ascribed to intermolecular force such as electrostatic attraction, Van der Waals attraction and so on.

FTIR spectroscopic analysis is performed to gain insight into RhB adsorption mechanisms on the surface of MoS_2. The FTIR spectra of MoS_2 before and after adsorption of RhB, with and without desorption, and crystalline RhB are shown in Fig. 5. The weak peaks at about 470 cm^{-1} at MoS_2 and MoS_2 after adsorption RhB FTIR spectra are assigned to Mo−S vibration.[31] While new peaks at about 1587 and 1340 cm^{-1} can be observed at the MoS_2 after adsorption RhB spectra, which are the characteristic of in-ring C−C and C−H stretching vibration in aromatic ring of pure RhB, respectively.[32] There is no obvious change in the intensity of RhB vibrations as compared to the FTIR spectra of MoS_2 after adsorption RhB with and without desorption, which indicates that the RhB has been tightly incorporated in MoS_2 backbone. Therefore, we believe that the electrostatic attraction could be responsible for RhB adsorption of MoS_2.

In order to confirm this conjecture, Methyl orange (MO), an anionic dye was used for comparative experiment. However, MO can not be removed from water by the flower-like MoS_2 (Fig. S1), which preferentially adsorb the cationic dye (RhB). The result indicated that the material could be potentially used for the separation and recycling of cationic and anionic dyes in the future.

4. Conclusions

In summary, flower-like MoS_2 nanostructures were successfully synthesized through a hydrothermal route by MoO_3 nanorods. The CV curves of the as-prepared MoS_2 nanoflowers possessed of a typical electrical double-layer capacitance with a high specific capacitance of 168 F g^{-1} at a current density of 1 A g^{-1} and after 3000 cycles still remain 92.6%. Beside the excellent electrochemical properties, the as-prepared MoS_2 nanoflowers also show good adsorption capacities on RhB solution and the maximum adsorption capacities of the flower-like MoS_2 is about 49.2 mg g^{-1}. Electrostatic attraction is responsible for RhB adsorption. All the data show that the flower-like MoS_2 can be suitable for electrochemical supercapacitor devices and also can be ideal adsorbent in water treatment.

Acknowledgements

References

1. K. Shiva, H. S. S. R. Matte, H. B. Rajendra, A. J. Bhattacharyya and C. N. R. Rao, *Nano Energy*, 2013, **2**, 787-793.
2. T. F. Jaramillo, K. P. Jorgensen, J. Bonde, J. H. Nielsen, S. Horch and I. Chorkendorff, *Science*, 2007, **317**, 100-102.
3. J.-Z. Wang, L. Lu, M. Lotya, J. N. Coleman, S.-L. Chou, H.-K. Liu, A. I. Minett and J. Chen, *Adv.Energy Mater.*, 2013, **3**, 798-805.
4. L. She, J. Li, D. Gu, Y. Shi, R. Che and D. Zhao, *Nanotechnology*, 2011, **22**, 075702.
5. B. Hinnemann, P. G. Moses, J. Bonde, K. P. Jorgensen, J. H. Nielsen, S. Horch, I. Chorkendorff and J. K. Norskov, *J. Am. Chem. Soc.*, 2005, **127**, 5308-5309.
6. Q. H. Wang, K. Kalantar-Zadeh, A. Kis, J. N. Coleman and M. S. Strano, *Nat. Nanotechnol.*, 2012, **7**, 699-712.
7. C. Zhu, X. Mu, P. A. van Aken, Y. Yu and J. Maier, *Angew. Chem. Int. Ed.*, 2014, **53**, 2152-2156.
8. J. Zheng, H. Zhang, S. Dong, Y. Liu, C. T. Nai, H. S. Shin, H. Y. Jeong, B. Liu and K. P. Loh, *Nat. Commun.*, 2014, **5**, 2995.
9. U. Maitra, U. Gupta, M. De, R. Datta, A. Govindaraj and C. N. R. Rao, *Angew. Chem. Int. Ed.*, 2013, **52**, 13057-13061.
10. L. Liao, J. Zhu, X. Bian, L. Zhu, M. D. Scanlon, H. H. Girault and B. Liu, *Adv. Funct. Mater.*, 2013, **23**, 5326-5333.
11. H. Li, X. Qi, J. Wu, Z. Zeng, J. Wei and H. Zhang, *ACS Nano*, 2013, **7**, 2842-2849.
12. X. Liu, M. Zheng, K. Xiao, Y. Xiao, C. He, H. Dong, B. Lei and Y. Liu, *Nanoscale*, 2014, **6**, 4598-4603.
13. D. J. Late, B. Liu, H. S. S. R. Matte, V. P. Dravid and C. N. R. Rao, *ACS Nano*, 2012, **6**, 5635-5641.
14. L. Zhang and X. W. Lou, *Chem. Eur. J.*, 2014, **20**, 5219-5223.
15. S. Ratha and C. S. Rout, *ACS Appl. Mat. Interfaces*, 2013, **5**, 11427-11433.
16. H. Pang, S. Wang, W. Shao, S. Zhao, B. Yan, X. Li, S. Li, J. Chen and W. Du, *Nanoscale*, 2013, **5**, 5752-5757.
17. G. Ma, H. Peng, J. Mu, H. Huang, X. Zhou and Z. Lei, *J. Power Sources*, 2013, **229**, 72-78.
18. M. Chhowalla, H. S. Shin, G. Eda, L.-J. Li, K. P. Loh and H. Zhang, *Nat. Chem.*, 2013, **5**, 263-275.
19. J. Feng, X. Sun, C. Wu, L. Peng, C. Lin, S. Hu, J. Yang and Y. Xie, *J. Am. Chem. Soc.*, 2011, **133**, 17832-17838.
20. L. Cao, S. Yang, W. Gao, Z. Liu, Y. Gong, L. Ma, G. Shi, S. Lei, Y. Zhang, S. Zhang, R. Vajtai and P. M. Ajayan, *Small*, 2013, **9**, 2905-2910.

21.   B. Lei, G. R. Li and X. P. Gao, *J. Mater. Chem. A*, 2014, **2**, 3919-3925.
22.   J. M. Soon and K. P. Loh, *Electrochem. Solid-State Lett.*, 2007, **10**, A250-A254.
23.   B. Hu, X. Qin, A. M. Asiri, K. A. Alamry, A. O. Al-Youbi and X. Sun, *Electrochim. Acta*, 2013, **100**, 24-28.
24.   K.-J. Huang, L. Wang, Y.-J. Liu, H.-B. Wang, Y.-M. Liu and L.-L. Wang, *Electrochim. Acta*, 2013, **109**, 587-594.
25.   K. Krishnamoorthy, G. K. Veerasubramani, S. Radhakrishnan and S. J. Kim, *Mater. Res. Bull.*, 2014, **50**, 499-502.
26.   X. Zhou, B. Xu, Z. Lin, D. Shu and L. Ma, *J. Nanosci. Nanotechnol.*, 2014, **14**, 7250-7254.
27.   P. Basnet and Y. Zhao, *J. Mater. Chem. A*, 2014, **2**, 911-914.
28.   J. Cao, J. Li, L. Liu, A. Xie, S. Li, L. Qiu, Y. Yuan and Y. Shen, *J. Mater. Chem. A*, 2014, **2**, 7953-7959.
29.   W. Zhou, Z. Yin, Y. Du, X. Huang, Z. Zeng, Z. Fan, H. Liu, J. Wang and H. Zhang, *Small*, 2013, **9**, 140-147.
30.   W. Yan, F. He, S. Gai, P. Gao, Y. Chen and P. Yang, *J. Mater. Chem. A*, 2014, **2**, 3605-3612.
31.   H. Akram, C. Mateos-Pedrero, E. Gallegos-Suarez, N. Allali, T. Chafik, I. Rodriguez-Ramos and A. Guerrero Ruiz, *J. Nanosci. Nanotechnol.*, 2012, **12**, 6679-6685.
32.   S. A. Hussain, S. Banik, S. Chakraborty and D. Bhattacharjee, *Spectrochim. Acta Part A*, 2011, **79**, 1642-1647.

Graphical Abstract
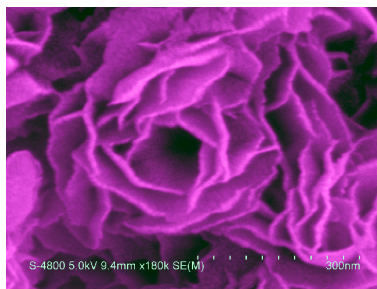
Uniform 3D flower-like MoS_2 nanostructures were successfully synthesized through a facile two-step hydrothermal method and had a high supercapacitor and adsorption behaviors toward Rhodamine B.

Figures Caption

Fig. 1 (a) SEM image of the precursor MoO_3 nanorods; (b) XRD pattern of the MoO_3 nanorods.

Fig. 2 (a, b) FESEM images of the flower-like MoS_2; (c) TEM of the flower-like MoS_2 and (d) XRD pattern of the MoS_2 sample.

Fig.3 (a) CV curves of MoS_2 electrode at various scan rates in 1M KCl; **(b)** Charge–discharge curves at a series of current densities for as-obtained MoS_2 electrode in 1M KCl; **(c)** Long-term stability curves of MoS_2 electrodes at a current density of 1 A g^{-1}; **(d)** The electrochemical impedance spectra of the electrodes at first and 100 cycles.

Fig.4 (a) UV–visible absorption spectra of 20 mg L^{-1} RhB solution at different absorption times with 0.02 g as-prepared MoS_2; **(b)** Adsorption rate curves of 0.02 g as-prepared MoS_2 in 20 mg L^{-1} RhB solution; **(c)** Adsorption isotherms of RhB solution using the as-prepared MoS_2 (C_e is the concentration of RhB, Q_e is the amount of RhB adsorbed per unit mass of adsorbent at equilibrium; **(d)** BET spectra of the as-obtained MoS_2; the inset shows the pore size distribution.

Scheme 1. Schematic illustration of the morphological evolution process of the MoS_2 nanostructures.

Fig.5 (a) FTIR spectra of MoS_2 before and after adsorption of RhB, with and without desorption, and crystalline RhB; **(b)** Enlarged image of the zone marked in (a).
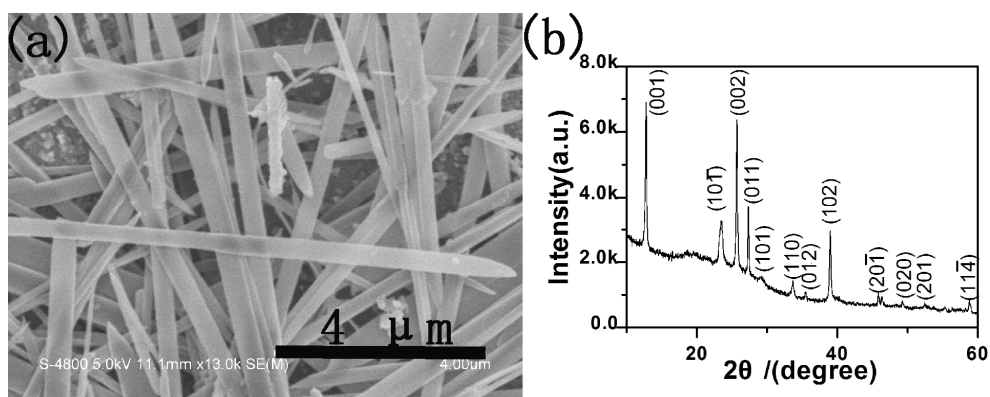
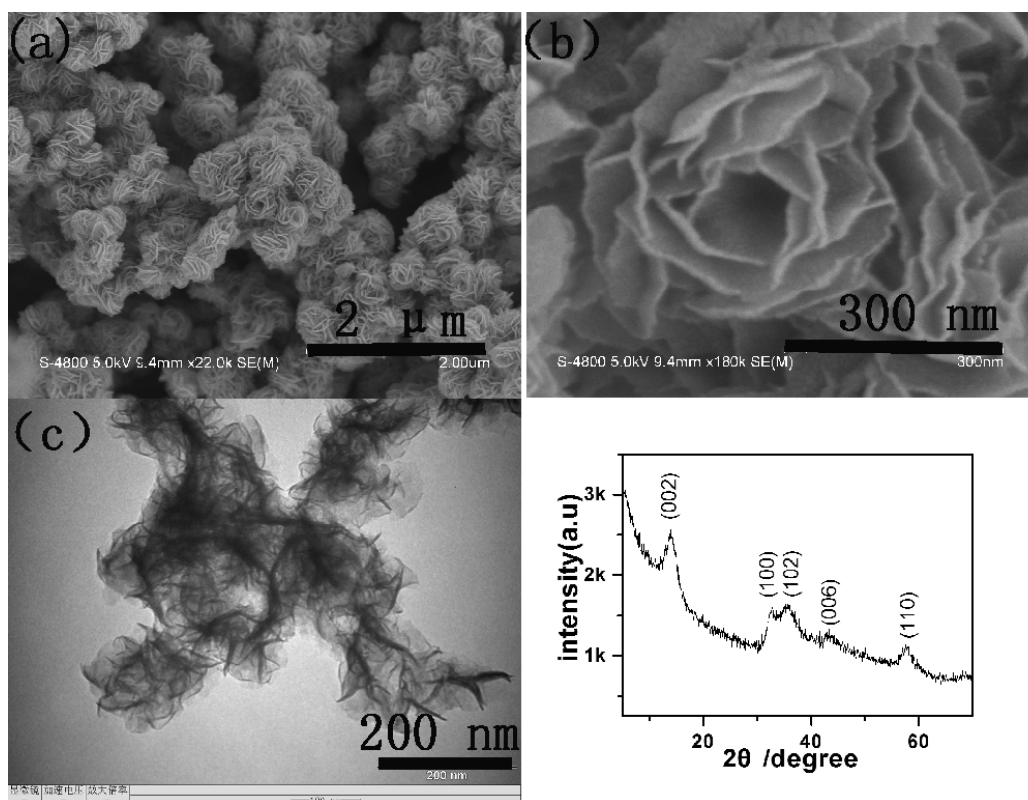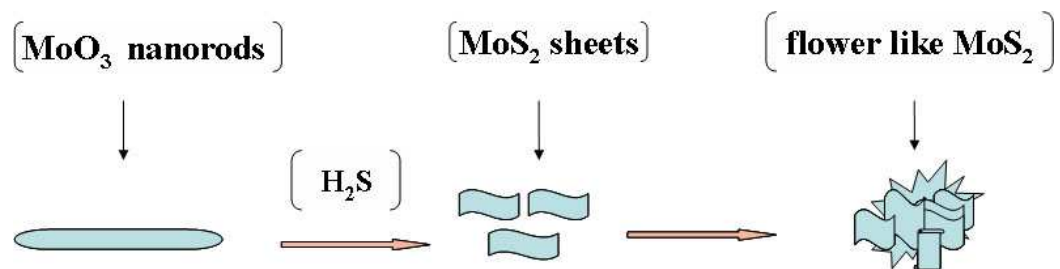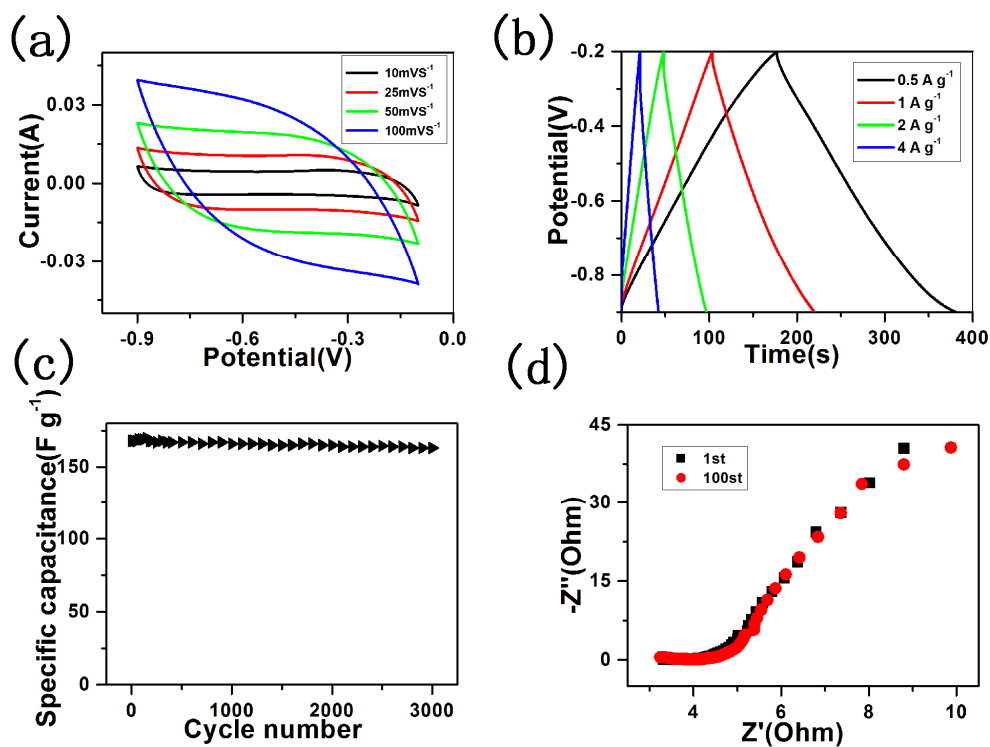**Fig. 1** (a) SEM image of the precursor MoO$_3$ nanorods; (b) XRD pattern of the MoO$_3$ nanorods.

Fig. 2 (a, b) FESEM images of the flower-like MoS$_2$; (c) TEM of the flower-like MoS$_2$ and (d) XRD pattern of the MoS$_2$ sample.

Scheme 1. Schematic illustration of the morphological evolution process of the MoS_2 nanostructures.

Fig.3 (a) CV curves of MoS_2 electrode at various scan rates in 1M KCl; **(b)** Charge–discharge curves at a series of current densities for as-obtained MoS_2 electrode in 1M KCl; **(c)** Long-term stability curves of MoS_2 electrodes at a current density of 1 A g^{-1}; **(d)** The electrochemical impedance spectra of the electrodes at first and 100 cycles.
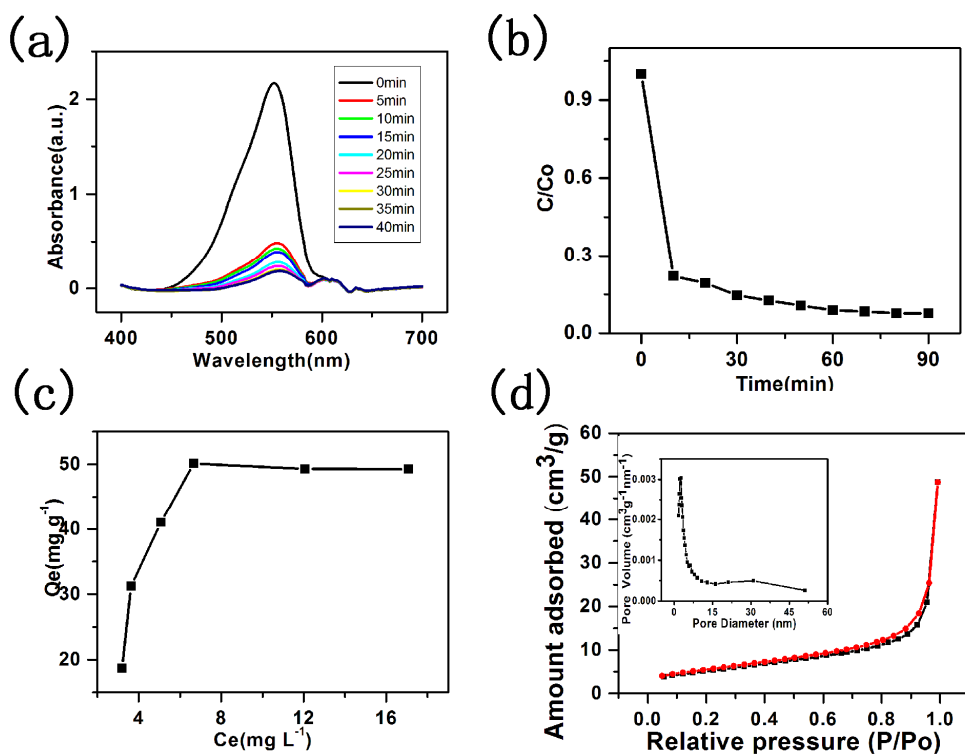
Fig.4 **(a)** UV–visible absorption spectra of 20 mg L^{-1} RhB solution at different absorption times with 0.02 g as-prepared MoS$_2$; **(b)** Adsorption rate curves of 0.02 g as-prepared MoS$_2$ in 20 mg L^{-1} RhB solution; **(c)** Adsorption isotherms of RhB solution using the as-prepared MoS$_2$ (C_e is the concentration of RhB, Q_e is the amount of RhB adsorbed per unit mass of adsorbent at equilibrium; **(d)** BET spectra of the as-obtained MoS$_2$; the inset shows the pore size distribution.
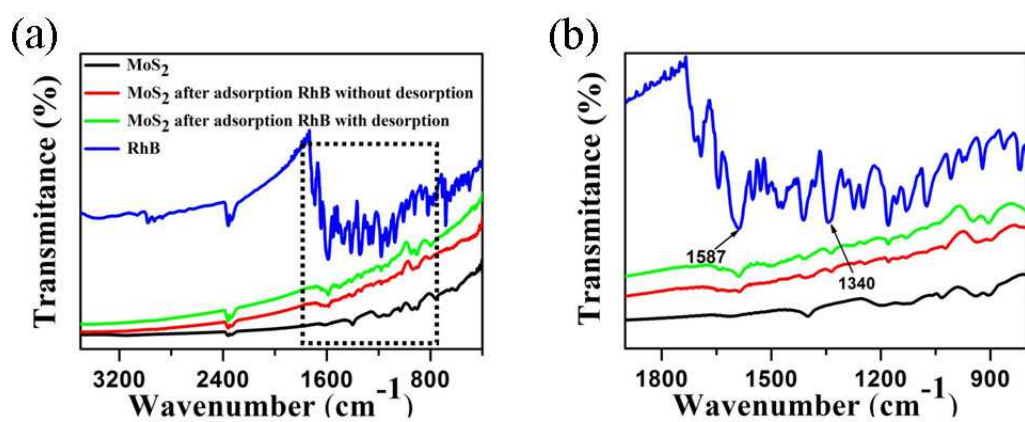
Fig.5 (a) FTIR spectra of MoS_2 before and after adsorption of RhB, with and without desorption, and crystalline RhB; **(b)** Enlarged image of the zone marked in (a).